Available online at www.sciencedirect.com
ScienceDirect
Journal of Power Sources 163 (2007) 1126–1131
JOURNAL OF POWER SOURCES
www.elsevier.com/locate/jpowsour

Short communication

# Anodic deposition of hydrous ruthenium oxide for supercapacitors

Chi-Chang Hu *, Ming-Jue Liu, Kuo-Hsin Chang

*Department of Chemical Engineering, National Chung Cheng University, Chia-Yi 621, Taiwan*

Received 28 July 2006; received in revised form 21 September 2006; accepted 27 September 2006
Available online 13 November 2006

**Abstract**

This communication demonstrates the success in the anodic deposition of hydrous ruthenium oxide (denoted as $RuO_2{\cdot}xH_2O$) from $RuCl_3{\cdot}xH_2O$ in aqueous media with/without adding acetate ions ($CH_3COO^-$, $AcO^-$) as the complex agent. The benefits of as-deposited $RuO_2{\cdot}xH_2O$ include the low electron-hopping resistance and the low contact resistance at the Ti-$RuO_2{\cdot}xH_2O$ interface which are clarified in electrochemical impedance spectroscopic (EIS) studies. The cycling stability, specific capacitance, and power performance of as-deposited $RuO_2{\cdot}xH_2O$ are further improved by annealing in air at 150 °C for 2 h. The morphologies of as-deposited and annealed $RuO_2{\cdot}xH_2O$ films, examined by scanning electron microscopy (SEM), are very similar to that of thermally decomposed $RuO_2$. The high onset frequencies of 660 and 1650 Hz obtained from EIS spectra for the as-deposited and annealed $RuO_2{\cdot}xH_2O$ films, respectively, definitely illustrate the high-power merits of both oxide films prepared by means of the anodic deposition without considering the advantages of its simplicity, one-step, reliability, low cost, and versatility for electrode preparation.
© 2006 Elsevier B.V. All rights reserved.

*Keywords:* Anodic deposition; Hydrous ruthenium oxide; Acetate ion; EIS analysis; Supercapacitors

## 1. Introduction

Electrochemical supercapacitors, with high-/pulse-power characteristics and longer cycle life time than rechargeable batteries, are an important energy storage device in the modern society. The integration of supercapacitors and batteries/fuel cells is believed to construct the energy storage systems of next generation, especially in the development of emission-free electrical vehicles (EVs). Based on the mechanisms of charge storage/delivery, supercapacitors can be divided into the electric double-layer capacitors (EDLCs) and pseudocapacitors [1,2]. Since the charge stored within the electric double layers is directly proportional to the electrolyte-accessible surface area of electrodes, materials with high specific area and inert to electrolytes are expected to be an ideal electrode material for EDLCs [3,4]. On the other hand, due to the extremely high reversibility of the superficial redox couples of certain electroactive materials, pseudocapacitors show a similar charge storage mechanism of rechargeable batteries but capacitive-like behavior. Moreover, several transition metal oxides [5–9] and conducting polymers [10,11] have been shown to exhibit pseudocapacitive behavior for this application.

Among the electroactive materials, $RuO_2$ in both amorphous and crystalline forms have been recognized as the most promising material due to the highly electrochemical reversibility, high specific capacitance, and excellent cycle life in $H_2SO_4$ [1,5,12]. Although the theoretic specific capacitance of hydrous ruthenium oxide ($RuO_2{\cdot}xH_2O$) is estimated to range from ca. 1300 to 2200 $F\,g^{-1}$ with various mean electron transfer numbers [13], a high specific capacitance value of 720 $F\,g^{-1}$ was obtained by the success in synthesizing $RuO_2{\cdot}xH_2O$ through a sol–gel method and a careful control of the annealing process in 1995 [5]. After this breakthrough, $RuO_2{\cdot}xH_2O$ was synthesized via various methods, including potentiodynamic deposition [14], electrostatic spray deposition [15], chemical precipitation of $RuO_2{\cdot}xH_2O$ colloids [16], solid-state reaction of $K_2CO_3$ and $RuO_2$ [17], oxidative synthesis [18], hydrothermal synthesis [19], and incipient wetness method [20]. All the above studies tried to gain a further understanding on the charge storage/delivery mechanism of $RuO_2{\cdot}xH_2O$, a better utilization of $RuO_2{\cdot}xH_2O$, or to develop simple, effective methods for synthesizing amorphous/crystalline $RuO_2$ for this application. Based on these studies, the key factors determining the capacitive performances (e.g., specific capacitance, cycle stability, power characteristics, etc.) of $RuO_2$-based supercapacitors have been discussed comprehensively [1,21,22].

* Corresponding author. Tel.: +886 5 2720411x33411; fax: +886 5 2721206.
*E-mail address:* chmhcc@ccu.edu.tw (C.-C. Hu).

0378-7753/$ – see front matter © 2006 Elsevier B.V. All rights reserved.
doi:10.1016/j.jpowsour.2006.09.060

Electrochemical deposition, having been considered as a simple, one-step, and cost-effective method, is much more advantageous than the other methods. For instance, the structure, surface morphology, and uniformity of oxides can be easily controlled by adjusting the parameters of electrochemical deposition such as the deposition mode, applied potential, current density, bath temperature, concentration of precursors, and addition of complex/additive agents [9,14,23,24]. Accordingly, electrochemical deposition of metal oxide films becomes an interesting and important research topic. In 1999, our group found that $RuO_2{\cdot}xH_2O$ can be directly deposited onto Ti substrates through a potential-cycling deposition method while the specific capacitance of this CV-deposited oxide is not high, probably due to the existence of Ru metal [14]. Thus, anodic deposition is believed to be an effective method to prepare $RuO_2{\cdot}xH_2O$ films without Ru metal. Unfortunately, investigations on the anodic deposition of $RuO_2{\cdot}xH_2O$ are very few although anodic deposition of transition metal oxides or hydroxides has been widely studied [9,25,26]. There is only one article employing anodic deposition for preparing $RuO_2{\cdot}xH_2O$ from an aqueous Ru(II) solution fabricated from an organo-metallic complex $[Ru(\eta^6\text{-}C_6H_6)Cl_2]_2$ [27]. In addition, it is not possible to directly deposit $RuO_2{\cdot}xH_2O$ onto graphite or carbon fabrics due to the oxidative attacks of Ru species in the higher oxidation state under an anodic, potentiostatic mode [28]. For a Ti substrate, a passive Ti oxide film will be formed at the interface between the Ti substrate and $RuO_2{\cdot}xH_2O$ under the anodic deposition process. This will significantly increase the contact resistance of electrodes although $RuO_2{\cdot}xH_2O$ can be directly deposited onto bare Ti. Accordingly, how to avoid the formation of this passive film at the Ti-$RuO_2{\cdot}xH_2O$ interface upon anodizing is also a serious issue. Based on the above viewpoints and facts, anodic deposition of $RuO_2{\cdot}xH_2O$ onto Ti from a simple $RuCl_3{\cdot}xH_2O$ aqueous solution is highly worthy being investigated. In addition, the ideal capacitive performances of this $RuO_2{\cdot}xH_2O$-coated Ti electrode clearly show the unique merits of this method.

## 2. Experimental

Hydrous ruthenium oxide films were directly electrodeposited onto Ti substrates in a potentiostatic mode. Prior to the deposition process, commercial 99% titanium substrates (10 mm × 10 mm × 0.5 mm) were mechanically polished by emery, which was blown by a high-pressure air compressor. These polished substrates were degreased with soap and water, and etched for 1.5 h in a 6 M HCl solution at ca. 90 °C. After the above cleaning steps, they were rinsed with water again and pickled for 10 min in a solution consisting of *N*,*N*-dimethylformamide (DMF, Wako E.P., Japan), water, and HF (Wako E.P.) in the volume ratio of 40:7.5:2.5. After the pickling pretreatment, the substrates were rinsed with acetone and water. Before anodic deposition, these pretreated Ti substrates were dip-coated with a very thin layer of $RuO_2{\cdot}xH_2O$ prepared by a hydrothermal synthesis method to prevent the formation of $TiO_2$ upon anodizing. These substrates were carefully coated with a thick film of PTFE with an exposed surface area of 1 $cm^2$, and then, $RuO_2{\cdot}xH_2O$ films were electroplated at 1.0 V from a 10 mM $RuCl_3{\cdot}xH_2O$ (Alfa Aesar) + 0.1 M NaAcO solution at 50 °C for various periods. After deposition, the PTFE film was removed and $RuO_2{\cdot}xH_2O$ deposits were repeatedly degreased with pure water and finally dried at room temperature under a reduced pressure. The weight of typical $RuO_2{\cdot}xH_2O$ films studied in this work is ca. 0.5–0.6 mg $cm^{-2}$, which can be easily controlled by varying the deposition time (and passed charge). After drying, these $RuO_2{\cdot}xH_2O$/Ti electrodes were coated with PTFE films to have an exposed surface area of 1 $cm^2$ for electrochemical characterization. The morphologies of $RuO_2{\cdot}xH_2O$ were observed using a field emission scanning electron microscope (Fe-SEM, Hitachi S4800 type I). The X-ray diffraction patterns were obtained from an X-ray diffractometer (multipurpose X-ray thin-film diffractometer, Shimadzu) using a Cu target (Cu Kα = 1.5418 Å) at 4° $min^{-1}$ ($2\theta$).

Electrochemical characteristics of $RuO_2{\cdot}xH_2O$/Ti electrodes were examined mainly by means of an electrochemical analyzer system, CHI 633A (CH Instruments, USA) in a three-compartment cell. The impedance spectrum analyzer, IM6 (ZAHNER), with the Thales software was employed to measure and analyze the EIS data. The potential amplitude of ac is equal to 10 mV meanwhile its frequency region is from 0.1 to 60 kHz. An Ag/AgCl electrode (Argenthal, 3 M KCl, 0.207 V versus SHE at 25 °C) was used as the reference and a piece of platinum gauze was employed as the counter electrode. A Luggin capillary was used to minimize errors due to *iR* drop in the electrolytes. All solutions used in this work were prepared with 18 MΩ cm water produced by a reagent water system (Milli-Q SP, Japan).

## 3. Results and discussion

Linear sweep voltammetry (LSV) was employed to illustrate the negative shift in the onset potential for the anodic deposition of $RuO_2{\cdot}xH_2O$ by adding the acetate ions into the deposition solution (see Fig. 1). Note that pH of all deposition solutions was adjusted to 2.5 before the LSV measurement. The

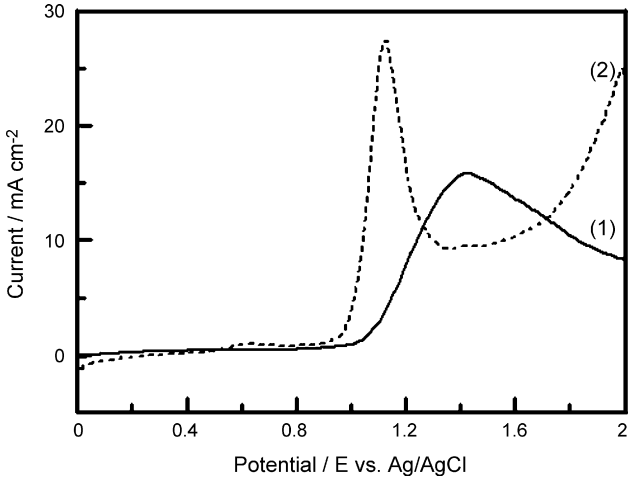


Fig. 1. Linear sweep voltammograms (LSV) measured at 10 mV $s^{-1}$ in 10 mM $RuCl_3{\cdot}xH_2O$ (1) without and (2) with 0.1 M NaOAc solutions at pH 2.5 and 50 °C.

oxidation of chloride precursor and the anodic deposition of $RuO_2{\cdot}xH_2O$ commence at ca. 1.0 V in the pure $RuCl_3{\cdot}xH_2O$ solution (curve 1). This reaction is under the diffusion control when the electrode potentials are behind 1.4 V. Surprisingly, the onset potential of $RuO_2{\cdot}xH_2O$ deposition is negatively shifted to 0.9 V when 0.1 M NaAcO has been added into the deposition solution (curve 2), and a very sharp peak corresponding to the deposition of $RuO_2{\cdot}xH_2O$ is located at about 1.1 V. This result suggests the formation of Ru–Cl–AcO complexes promoting the deposition rate of $RuO_2{\cdot}xH_2O$. Since a more obvious negative shift in the onset potential for the anodic deposition of $MnO_2{\cdot}xH_2O$ with the presence of $AcO^-$ was also found in our previous work [29] and since a sharp peak is found on curve 2 in Fig. 1, the presence of $AcO^-$ is believed to alter the anodic deposition mechanism of $RuO_2{\cdot}xH_2O$. As mentioned in Section 1, $RuO_2{\cdot}xH_2O$ cannot be directly deposited onto carbon due to oxidative attack under the anodic, potentiostatic modes [28]. The above negative shift on the onset potential and the enhanced deposition rate of $RuO_2{\cdot}xH_2O$ reduce the oxidative attack to carbon. Therefore, $RuO_2{\cdot}xH_2O$ can be easily electroplated onto active carbon, graphite or carbon nanotubes under anodic deposition. It has to be emphasized here that the presence of $AcO^-$ in the precursor solutions does not always change the deposition mechanism of transitional metal oxides from our unpublished data. For example, the onset potential for the anodic deposition for Ni oxide was found to be independent of adding $AcO^-$ in various $Ni^{2+}$ aqueous solutions. In addition, from the different effects of adding $AcO^-$ on the deposition behavior of $MnO_2{\cdot}xH_2O$ and $RuO_2{\cdot}xH_2O$, the influences of complex agents on the deposition mechanism are believed to be very complicated.

The porous nature of as-deposited and annealed $RuO_2{\cdot}xH_2O$ films was examined by means of scanning electron microscopy (SEM, see Fig. 2b and c), which is very different from the HF-etched, rough surface of a Ti substrate shown in Fig. 2a. The as-deposited and annealed $RuO_2{\cdot}xH_2O$ show "mud-cracked" morphologies while cracks on the $RuO_2{\cdot}xH_2O$ film become clear and large, and the surface of $RuO_2{\cdot}xH_2O$ grains becomes relatively smooth after annealing. The presence of cracks suggests the existence of inner stress in the deposit while the relatively smooth surface is believed to result from the coalescence of $RuO_2{\cdot}xH_2O$ particulates in the film during the annealing process. This coalescence of $RuO_2{\cdot}xH_2O$ particulates can be effectively inhibited by the formation of $RuO_2{\cdot}xH_2O$ nanocrystallites synthesized through a hydrothermal method [30]. Note that the surface morphologies of as-deposited and annealed $RuO_2{\cdot}xH_2O$ films are very similar to that of dimensionally stable anodes (DSA) prepared by thermal decomposition [31]. This porous, cracked nature was also proposed to be favorable for the penetration of electrolytes [31,32], resulting in a better utilization of active species (see below).

The capacitive behavior of the as-deposited $RuO_2{\cdot}xH_2O$/Ti electrode, examined by cyclic voltammetry (CV) in 0.5 M $H_2SO_4$ at 25 mV $s^{-1}$ (see Fig. 3a), exhibits the typical responses of $RuO_2{\cdot}xH_2O$ with high water content, i.e., relatively low capacitive currents are found in the less positive potential region [5,13,16,18]. A significant decay in the voltammetric currents

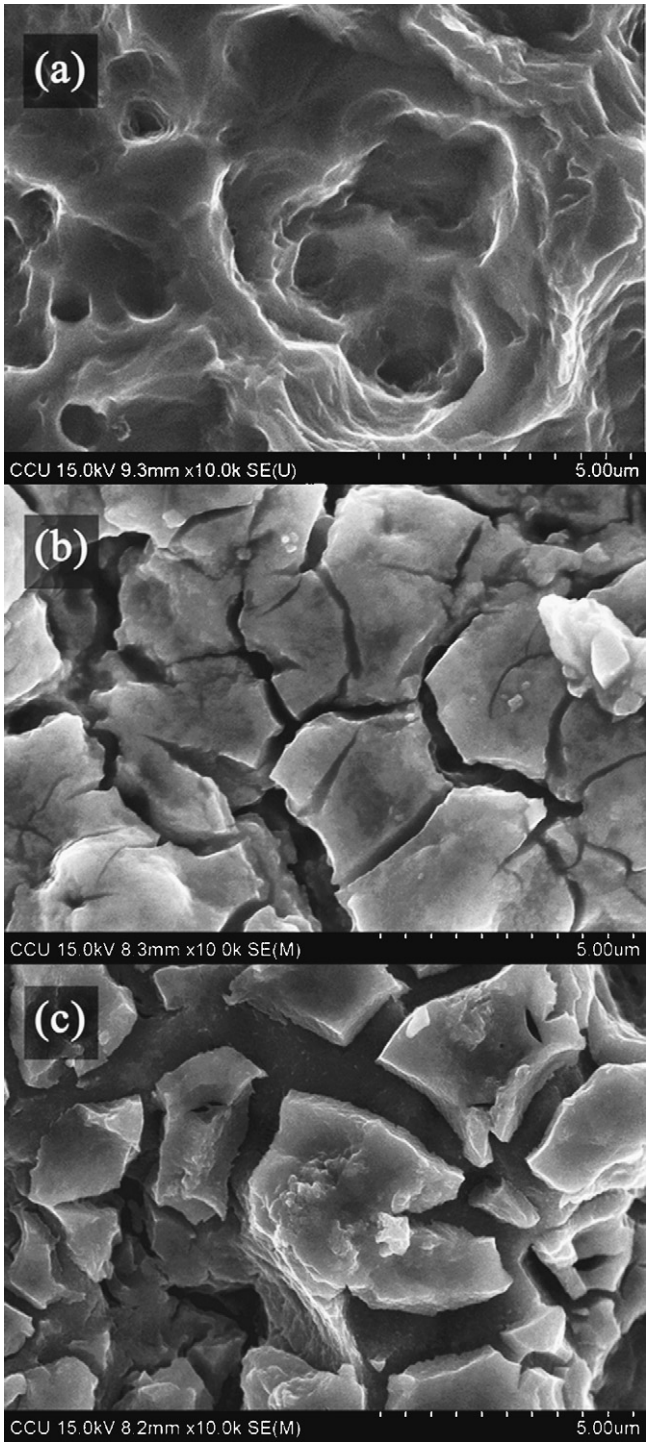


Fig. 2. SEM surface morphologies of (a) a Ti substrate, (b) an as-deposited $RuO_2{\cdot}xH_2O$/Ti electrode and (c) with annealing in air at 150 °C for 2 h.

is clearly found with the repeated applications of CV, indicating that the stability of as-deposited $RuO_2{\cdot}xH_2O$ are relatively poor in the CV test. However, the cycling stability of as-deposited $RuO_2{\cdot}xH_2O$ film is significantly improved by the annealing application at 150 °C in air for 2 h since the CV curves of this annealed $RuO_2{\cdot}xH_2O$/Ti electrode, shown in Fig. 3b, are completely overlapped. In addition, the positive sweeps show almost mirror images of their corresponding negative sweeps

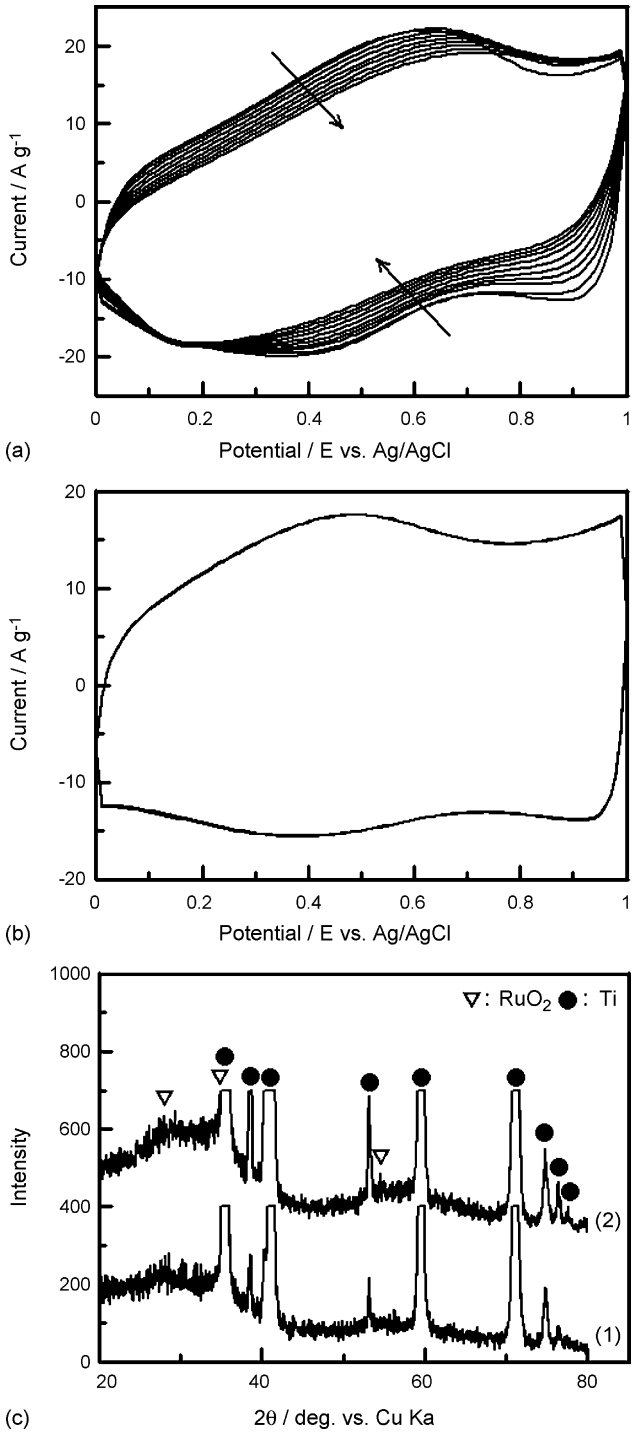


Fig. 3. (a and b) Cyclic voltammograms and (c) XRD patterns of (a, 1) as-deposited and (b, 2) annealed $RuO_2{\cdot}xH_2O$/Ti electrodes measured at 25 mV $s^{-1}$ in 0.5 M $H_2SO_4$.

for this annealed $RuO_2{\cdot}xH_2O$/Ti electrode and obvious pseudocapacitive currents are found on both positive and negative sweeps from 0 to 0.5 V. Both results reveal the ideal capacitive behavior of $RuO_2{\cdot}xH_2O$ annealed at 150 °C. Moreover, the specific capacitance of $RuO_2{\cdot}xH_2O$ (measured at 25 mV $s^{-1}$) is increased from 460 to 552 F $g^{-1}$, indicating a better utilization of active species. The above transformation in the *i–E* responses and the increase in the specific capacitance are attributable to the

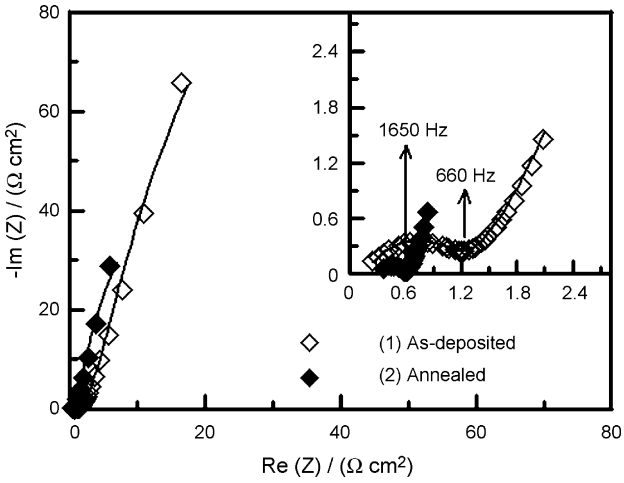


Fig. 4. Nyquist plots for (1) as-deposited and (2) annealed $RuO_2{\cdot}xH_2O$/Ti electrodes measured at 0.2 V in 0.5 M $H_2SO_4$. *Inset*: Data in the high-frequency region.

improvement in the electronic conductivity of Ru oxide upon annealing [5,13,33].

As mentioned in Section 1, the specific capacitance of a CV-deposited $RuO_2{\cdot}xH_2O$ film is not very high, probably due to the existence of Ru metal [14] and the purpose of using anodic deposition is to prepare $RuO_2{\cdot}xH_2O$ films without Ru metal. This idea is strongly supported by the much higher specific capacitance (460 F $g^{-1}$) of $RuO_2{\cdot}xH_2O$ prepared by the anodic deposition (in comparison with the CV-deposited $RuO_2{\cdot}xH_2O$ with ~100 F $g^{-1}$) as well as the absence of diffraction peaks corresponding to Ru metal on the XRD patterns shown in Fig. 3c. The absence of Ru metal is easily understood since the Ru precursor employed in this work is Ru(III) species which will be oxidized into a higher oxidation state, such as $RuO_2$, in an anodic process.

The EIS analysis, representing as the Nyquist plots (see Fig. 4), is used to clarify the unique capacitive characteristics of $RuO_2{\cdot}xH_2O$ prepared by anodic deposition. From curve 1 in Fig. 4, the equivalent series resistance (ESR), estimated from the diameter of the impedance arc in the high-frequency region, for the as-deposited $RuO_2{\cdot}xH_2O$/Ti electrode is much smaller than that of single-crystalline $RuO_2$ nanorods prepared CVD [34]. In the medium frequency region, the "onset" frequency for the as-deposited electrode behaving as a capacitor is located at ca. 660 Hz, which is much higher than that of hydrothermal derived $RuO_2{\cdot}xH_2O$ nanoparticles [19] or single-crystalline $RuO_2$ nanorods prepared by CVD [34]. In this work, the onset frequency is defined as the frequency where the lowest image impedance occurs or the frequency where the impedance starts to be dominated by the image (capacitor) part in the medium frequency region. Hence, the electroactive materials are considered to behave as a capacitor behind this frequency and the higher the onset frequency of an electrode material is, the higher power density for this material can be achieved. The high onset frequency (660 Hz) of as-deposited $RuO_2{\cdot}xH_2O$ reveals its high-power characteristics.

From a comparison of EIS spectra shown in Fig. 4, three features have to be mentioned. First, the impedance of the

annealed $RuO_2{\cdot}xH_2O$/Ti electrode (i.e., curve 2) in the image part measured at any specified frequency is smaller than that of the as-deposited film (i.e., curve 1). This result indicates the higher specific capacitance of the annealed $RuO_2{\cdot}xH_2O$/Ti electrode, which is consistent with the CV results. Second, the ESR is also smaller for the annealed electrode, indicative of the significant improvement in the electronic conductivity of the annealed oxide. Third, the onset frequency of the as-deposited electrode is obviously shifted from 660 to 1650 Hz upon annealing. All the above results reveal the significant improvement in the capacitive performances of $RuO_2{\cdot}xH_2O$ through annealing, which was commonly found previously [5,6,13,21,22,33,35]. In addition, the high onset frequency of as-deposited $RuO_2{\cdot}xH_2O$ indicates the low ESR resulting from the simultaneous reduction in "between-particle" and "in-particle" electron-hopping resistances as well as the contact resistance at the Ti-$RuO_2{\cdot}xH_2O$ interface [21,22], which is the main benefit of this anodic deposition process. Similar phenomena are also found for the EIS spectra measured at 0.6 V (not shown here), which were also found previously [35]. This indicates that both as-prepared and annealed $RuO_2{\cdot}xH_2O$ show the excellent capacitive responses in the whole potential region of investigation.

Since the impedance spectra of both as-deposited and annealed $RuO_2{\cdot}xH_2O$ are very analogous to the Nyquist plots reported previously [35], the impedance data can be analyzed by using the same circuit model through an assumption that the impedance behavior is dominated by three major processes occurring in the high, medium, and low frequency regions, respectively [35]. Qualitatively, the high-frequency impedance arc is attributable to the processes occurring at the composite–electrolyte interface. When the frequency passes the onset frequency, a curve with its slope gradually changing from ca. 45° to 90° represents the finite-length diffusion Warburg behavior which ascribes the impedance due to highly distributed proton diffusion within $RuO_2{\cdot}xH_2O$ in the medium frequency region [35]. In the relatively low frequency region, a quasi-vertical line, representing pseudocapacitive behavior, clearly confirms their excellent capacitive responses.

The specific power (SP) and specific energy (SE) of $RuO_2{\cdot}xH_2O$ can be deduced from the EIS spectra since the dependence of specific capacitance of active materials on the applied ac frequency can be estimated from the EIS spectra [35]. When the applied frequency is equal to 1 Hz (i.e., 1 cycle per second), the equivalent scan rate of CV should be equal to $40\,mV\,s^{-1}$ because the amplitude of ac in this study is 10 mV. Thus, SE and SP of active materials can be evaluated on the basis of the following equations:

$$SE = \frac{\Delta VQ}{2w} = \frac{C_s(\Delta V)^2}{2} \quad (1)$$

$$SP = \frac{\Delta Vi}{2w} = \frac{\Delta VC_s\nu}{2} \quad (2)$$

where $\Delta V = 1$ V, $C_s$ is estimated from EIS spectra and $\nu$ is the scan rate of CV deduced from the ac frequency (e.g., $100\,Hz = 4000\,mV\,s^{-1}$). Note the ultrahigh SP of annealed $RuO_2{\cdot}xH_2O$ (about $147\,kW\,kg^{-1}$) since $C_s$ deduced from curve 2 in Fig. 4 at 100 Hz is about $73.5\,F\,g^{-1}$ [35]. In addition, the average SP and $C_s$ of $RuO_2{\cdot}xH_2O$ obtained from a CV curve measured at a compatible scan rate of $4000\,mV\,s^{-1}$ are equal to ca. $224\,kW\,kg^{-1}$ and $112\,F\,g^{-1}$, respectively ($170\,kW\,kg^{-1}$ and $340\,F\,g^{-1}$ at $1000\,mV\,s^{-1}$) which are larger than that derived from EIS data. This effect has been found previously [1], indicating that the behavior of $RuO_2{\cdot}xH_2O$ under ac modulation exhibits a dispersion of capacitance, i.e., the accessible capacitance of this $RuO_2{\cdot}xH_2O$/Ti electrode is frequency-dependent.

## 4. Conclusions

In this communication, a simple, one-step, cost-effective method, i.e., anodic deposition of $RuO_2{\cdot}xH_2O$ onto Ti from a simple chloride precursor solution, is successfully demonstrated. The presence of $AcO^-$ in the aqueous $RuCl_3{\cdot}xH_2O$ solution obviously promotes the rate of $RuO_2{\cdot}xH_2O$ deposition from the negative shift in the onset potential and the presence of a sharp peak, which definitely reduce the oxidative attack to carbon. The as-deposited $RuO_2{\cdot}xH_2O$/Ti electrode shows the merit of low ESR (i.e., high electronic conductivity and low contact resistance at the interface between Ti and $RuO_2{\cdot}xH_2O$) through the EIS analysis. The cycling stability, specific capacitance (increasing from 460 to $552\,F\,g^{-1}$), and power performance of as-deposited $RuO_2{\cdot}xH_2O$ are significantly improved by annealing in air at 150 °C for 2 h. The significant reduction in the ESR through annealing extends the onset frequency from 660 to 1650 Hz for $RuO_2{\cdot}xH_2O$ behaving as a capacitor, which is much higher than that of hydrothermal-derived $RuO_2{\cdot}xH_2O$ nanocrystallites or single-crystalline $RuO_2$ nanorods prepared by CVD, illustrating its ultrahigh power characteristics ($\sim 147\,kW\,kg^{-1}$ at 100 Hz).

## Acknowledgment

The financial support of this work, by the National Science Council of the Republic of China under contract no. NSC 94-2214-E-194-003, is gratefully acknowledged.

## References

[1] B.E. Conway, Electrochemical Supercapacitors, Kluwer-Plenum, New York, 1999.
[2] R. Kotz, M. Carlen, Electrochim. Acta 45 (2000) 2483.
[3] E. Frackowiak, F. Beguin, Carbon 39 (2001) 937.
[4] C. Niu, E.K. Sichel, R. Hoch, D. Moy, H. Tennent, Appl. Phys. Lett. 70 (1997) 1480.
[5] J.P. Zheng, P.J. Cygan, T.R. Jow, J. Electrochem. Soc. 142 (1995) 2699.
[6] C. Lin, J.A. Ritter, B.N. Popov, J. Electrochem. Soc. 145 (1998) 4097.
[7] H.Y. Lee, J.B. Goodenough, J. Solid State Chem. 148 (1999) 81.
[8] N.L. Wu, S.Y. Wang, C.Y. Han, D.S. Wu, L.R. Shiue, J. Power Sources 113 (2003) 173.
[9] C.C. Hu, T.W. Tsou, Electrochem. Commun. 4 (2002) 105.
[10] S. Ghosh, O. Inganas, Adv. Mater. 11 (1999) 1214.
[11] V. Gupta, N. Miura, Electrochem. Solid-State Lett. 8 (2005) A630.
[12] S. Hadzi-Jordanov, H. Angerstein-Kozlowska, M. Vukovic, B.E. Conway, J. Electrochem. Soc. 125 (1978) 1471.
[13] C.C. Hu, W.C. Chen, K.H. Chang, J. Electrochem. Soc. 151 (2004) A281.
[14] C.C. Hu, Y.H. Huang, J. Electrochem. Soc. 146 (1999) 2465.
[15] I.H. Kim, K.B. Kim, Electrochem. Solid-State Lett. 4 (2001) A62.

[16] H. Kim, B.N. Popov, J. Power Sources 104 (2002) 52.
[17] W. Sugimoto, H. Iwata, Y. Yasunaga, Y. Murakami, Y. Takasu, Angew. Chem. Int. Ed. 42 (2003) 4092.
[18] K.H. Chang, C.C. Hu, J. Electrochem. Soc. 151 (2004) A958.
[19] K.H. Chang, C.C. Hu, Electrochem. Solid-State Lett. 7 (2004) A466.
[20] M. Min, K. Machida, J.H. Jang, K. Naoi, J. Electrochem. Soc. 153 (2006) A334.
[21] C.C. Hu, Invited Lecture in the 56th Annual Meeting of ISE (3C-013-IL), Busan, Korea, September 26–30, 2005.
[22] K.H. Chang, Y.T. Wu, C.C. Hu, Key factors determining the performances of $RuO_2$-based supercapacitors, in: V. Gupta (Ed.), Recent Advances in Supercapacitors, Chapter 3, Transworld Research Network, Kerala, India, 2006, pp. 29–56.
[23] K.R. Prasad, N. Miura, Appl. Phys. Lett. 85 (2004) 4199.
[24] M.S. Wu, Appl. Phys. Lett. 87 (2005) 153102.
[25] C.C. Hu, C.Y. Cheng, J. Power Sources 111 (2002) 137.
[26] T.C. Wen, M.G. Wei, K.-L. Lin, J. Electrochem. Soc. 137 (1990) 2700.
[27] D.P. Anderson, L.F. Warren, J. Electrochem. Soc. 131 (1984) 347.
[28] C.C. Wang, C.C. Hu, Carbon 43 (2005) 1926.
[29] C.C. Hu, P.Y. Chuang, Y.T. Wu, J. Electrochem. Soc. 152 (2005) C723.
[30] K.H. Chang, C.C. Hu, Appl. Phys. Lett. 88 (2006) 193102.
[31] S. Trasatti (Ed.), Electrodes of Conductive Metallic Oxides, Part A and Part B, Elsevier, Amsterdam, 1980–1981.
[32] J. Gaudet, A.C. Tavares, S. Trasatti, D. Guay, Chem. Mater. 17 (2005) 1570.
[33] D.A. McKeown, P.C. Hagans, L.P.L. Carette, A.E. Russell, K.E. Swider, D.R. Rolison, J. Phys. Chem. B 103 (1999) 4825.
[34] Y.F. Ke, D.S. Tsai, Y.S. Huang, J. Mater. Chem. 15 (2005) 2122.
[35] W. Sugimoto, H. Iwata, K. Yokoshima, Y. Murakami, Y. Takasu, J. Phys. Chem. B 109 (2005) 7330.